Constraining the temporal variations of Ra isotopes and Rn in the groundwater end-member: Implications for derived SGD estimates

Marc Cerdà-Domènech[a,*], Valentí Rodellas[b,c], Albert Folch[d,e], Jordi Garcia-Orellana[b,f]

(a) GRC Geociències Marines, Dep. de Dinàmica de la Terra i de l'Oceà, Universitat de Barcelona, 08028 Barcelona, Spain.

(b) Institut de Ciència i Tecnologia Ambientals (ICTA), Universitat Autònoma de Barcelona, 08193 Bellaterra, Spain.

(c) Center de Recherche et d'Enseignement de Géosciences de l'Environment (CEREGE), Aix-Marseille Université, 13545 Aix-en-Provence, France.

(d) Department of Civil and Environmental Engineering, Universitat Politècnica de Catalunya (UPC), c/Jordi Girona 1-3, Barcelona, Spain

(e) Associated Unit: Hydrogeology Group (UPC-CSIC), Spain

(f) Departament de Física, Universitat Autònoma de Barcelona, 08193 Bellaterra, Spain.

*Corresponding author:

Marc Cerdà-Domènech

GRC Geociències Marines, Departament de Dinàmica de la Terra i de l'Oceà

Facultat de Ciències de la Terra, Universitat de Barcelona

c/ Martí Franquès s/n, 08028, Barcelona, Spain

Tel.: (+34) 93 402 13 69 Fax: (+34) 93 402 13 40

E-mail: cerda.domenech@ub.edu

KEYWORDS: submarine groundwater discharge, radium, radon, salinity interface, end-member

Highlights:

1. Ra isotopes and ^{222}Rn were measured for nearly two years in a coastal piezometer.
2. High Ra variability was registered, especially during intense rainfall events.
3. ^{222}Rn displayed minor variations due to the no influence of groundwater salinity on radon emanation.
4. The hydrodynamics of coastal aquifers must be considered as essential to understand SGD fluxes.

ABSTRACT

Submarine groundwater discharge (SGD) has been recognized as an important supplier of chemical compounds to the ocean that may influence coastal geochemical cycles. Radium isotopes (^{223}Ra, ^{224}Ra, ^{226}Ra, ^{228}Ra) and radon (^{222}Rn) have been widely applied as tracers of SGD. Their application requires the appropriate characterization of both the concentrations of tracers in the discharging groundwater and their distribution in the coastal water column. This study evaluates the temporal evolution of Ra isotopes and ^{222}Rn concentrations in a dynamic subterranean estuary of a microtidal Mediterranean coastal aquifer that experiences large displacements of the fresh-saltwater interface as a necessary initial step in evaluating the influence of SGD in coastal waters. We show that changes in groundwater salinities due to the seaward displacement of the fresh-saltwater interface produced large variations in Ra activities in groundwater (by a factor of ~19, ~14, ~6, and ~11 for ^{223}Ra, ^{224}Ra, ^{226}Ra and ^{228}Ra, respectively), most importantly during rainfall events. In contrast, the ^{222}Rn activities in groundwater oscillated by a factor of 3 during these rainy periods. The large temporal variability in Ra activities hampers characterization of the SGD end-member when using Ra isotopes as tracers, and thus presents a challenge for obtaining accurate SGD estimates. This study emphasizes the need to understand the hydrodynamics of coastal aquifers to appropriately constrain the Ra isotopes and ^{222}Rn concentrations in groundwater and when applying both tracers in dynamic microtidal coastal systems.

56 1. INTRODUCTION

57 Submarine Groundwater Discharge (SGD) includes both meteoric fresh groundwater flowing
58 into the sea and seawater recirculation through coastal aquifers (Burnett et al., 2003). Both
59 flows mix in coastal aquifers, so-called subterranean estuaries (STEs), where biogeochemical
60 reactions occur as a consequence of interactions between terrestrially derived groundwater,
61 recirculated seawater and the geological matrix (Moore, 1999). This dynamic mixing zone
62 influences the transfer of several chemical constituents to the coastal ocean (Tovar-Sánchez et
63 al., 2014; Sadat-Noori et al., 2016). SGD is now recognized as a relevant source of nutrients,
64 trace metals and other compounds and contaminants to the coastal sea (Kim et al., 2003;
65 Johnson et al., 2008; Gonneea et al., 2014; Pavlidou et al., 2014; Rodellas et al., 2015b; Trezzi
66 et al., 2016)

67 Radium (Ra) isotopes (^{223}Ra, ^{224}Ra, ^{226}Ra, ^{228}Ra) and radon (^{222}Rn) have been widely used as
68 tracers to quantify SGD (e.g., Charette et al., 2001; Moore, 2003; Burnett et al., 2006, Burnett et
69 al., 2008; Lee et al., 2012). Ra isotopes and ^{222}Rn, which are continuously produced in geological
70 materials by the decay of their uranium and thorium parents, are appropriate SGD tracers, mainly
71 because they behave conservatively once released to the sea and because they are significantly
72 enriched in SGD fluids relative to seawater (Burnett et al., 2006). The approach used to estimate
73 SGD flows using Ra isotopes or ^{222}Rn is based on characterizing the flux of Ra/Rn supplied by
74 SGD (J_{Ra} or J_{Rn}) using the Ra/Rn distribution in coastal waters and the Ra/Rn concentration in
75 groundwater inflowing to the sea, the so-called SGD end-member (Ra_{GW} or Rn_{GW}) (Burnett and
76 Dulaiova, 2003; Moore, 1996a).

77 Most SGD studies have been devoted primarily to estimating the fluxes of Ra and Rn (J_{Ra} or J_{Rn})
78 (e.g., Kim et al., 2005; Beck et al., 2008; Smoak et al., 2012), whereas the Ra and Rn
79 concentrations in the groundwater end-member have been largely overlooked, even though they
80 are a critical component of the tracer-derived estimates (Cho and Kim, 2016; Burnett et al., 2007;
81 Gonneea et al., 2013, 2008). Ra activities in subterranean estuaries can vary significantly (one or
82 two orders of magnitude) over space and time at a given study site (Ollivier et al., 2007; Beck et

al., 2008). Thus, the lack of constraint on this term remains a significant source of uncertainty in Ra-derived SGD estimates (Charette, 2007; Gonneea et al., 2013).

Several factors influence Ra activities in SGD, including the presence of Mn-Fe oxides (Gonneea et al., 2008), the pH of the subterranean estuary (Beck and Cochran, 2013), the ionic strength (Elsinger and Moore, 1980; Webster et al., 1995), the properties of the geological matrix (Swarzenski, 2007) and the residence time within the STE (Rodellas et al., 2017). Among them, the ionic strength of the solution (i.e., its salinity) has long been recognized as the main factor influencing the Ra activities in the SGD end-member, and Ra desorption increases significantly with salinity (Cho and Kim, 2016; Elsinger and Moore, 1980; Webster et al., 1995). As a consequence, Ra activities in SGD may vary substantially depending on the position of the freshwater-saltwater interface within the subterranean estuary. The position of this interface may oscillate, due to variations in the hydraulic gradient of the fresh groundwater (caused by, e.g., recharge and abstraction) and marine driving forces (e.g., tides, wave and storms) (Gonneea et al., 2013; Heiss and Michael, 2014). These temporal oscillations of Ra activity in STEs, along with the spatial heterogeneity of coastal aquifers, make it difficult to characterize the Ra_{GW} end-member, which is needed to provide accurate estimates of SGD (Michael et al., 2011).

Unlike Ra, Rn is an inert gas. Thus, its chemical behavior is not influenced by the physicochemical characteristics of the coastal aquifer (e.g., groundwater salinity, temperature or redox conditions). Radon activities in coastal aquifers are thus primarily controlled by the content of ^{226}Ra in the aquifer solids and dissolved in groundwater (Dulaiova et al., 2008). However, the physical and geochemical processes occurring in coastal aquifers (e.g., manganese cycling or ionic exchange) can affect the ^{226}Ra distribution, thus driving changes in the ^{222}Rn concentration of groundwater (Dulaiova et al., 2008).

In contrast to many coastal areas of the world, the Mediterranean Sea is characterized by a microtidal regime, with tidal amplitudes commonly lower than 0.2 m. Therefore, tidal forces do not exert a significant water pumping influence in the coastal aquifers there. As a consequence, the location and movement of the salinity interface in subterranean estuaries in the Mediterranean region, as well as in other microtidal sea regions (e.g., the Caribbean Sea or the Baltic Sea), are

mainly regulated by hydrogeological factors, such as aquifer properties and the aquifer water budget. Thus, understanding the hydrogeological characteristics (i.e. recharge, discharge, etc.) of coastal aquifers in microtidal regions and their impacts on the Ra and Rn concentrations in groundwater is particularly important for improving tracer-derived estimates of SGD.

This study evaluates the temporal evolution of Ra isotopes and ^{222}Rn concentrations in a Mediterranean microtidal coastal aquifer (Argentona, Catalonia, Eastern Iberian Peninsula) over almost 2 years. During this period, two piezometers (PZ) were continuously monitored to measure variations in groundwater levels, salinity and the Ra and ^{222}Rn concentrations in the groundwater. The aim of this study is to assess hydrogeological dynamics affecting the variability in the concentrations of Ra isotopes and ^{222}Rn in groundwater from this coastal microtidal aquifer. This variability may have critical implications for the quantification of Ra/Rn-derived SGD fluxes and therefore their implications for coastal biogeochemical cycles.

2. STUDY AREA AND METHODS

2.1 Study area: The Argentona alluvial aquifer and the oceanographic setting

The Argentona alluvial aquifer is located between the Catalan Littoral Mountain Range and the Mediterranean Sea (Barcelona, NW Mediterranean) and extends in the SW-NE direction (Figure 1). It has an area of approximately 35 km^2 that is mainly devoted to agricultural uses. The climatology of this region is characterized by Western Mediterranean conditions, and the region experiences high temperatures in summer (mean ~23 °C) and mild temperatures in winter (mean ~10 °C). The annual precipitation of the area ranges from 500 to 800 mm, and is mainly related to intense and short storms during the fall and spring season. Surface water flows in the Argentona main stream are restricted to the rainy seasons, particularly during major rainfall events (e.g., > 50 mm in a few hours).

The Argentona aquifer is associated with a tectonic fault and sinking blocks where stream valleys have developed. The geology of the alluvial aquifer, which is unconfined, is dominated by detrital Quaternary sediments that are the product of chemical weathering of the granitic basement along

fissures (Montoto, 1967). These sediments constitute layers of unconsolidated sands, gravels and clays deposited in an alluvial fan system during basin formation. In the nearshore area, the aquifer is mainly composed of marine sands (Catalan Water Agency, 2010).

A water budget for the aquifer conducted by the Catalan Water Agency (ACA), which used a numerical flow model of the aquifer system and covered the period 2006-2009, estimated an aquifer recharge rate between $3.6 \cdot 10^6$ to $5.4 \cdot 10^6$ $m^3 y^{-1}$. Major outputs from the aquifer include urban, agricultural and industrial extraction ($(1.4 - 1.9) \cdot 10^6$ m^3 y^{-1}) and fresh groundwater discharge to the sea ($(1.2 - 2.4) \cdot 10^6$ $m^3 y^{-1}$).

2.2 Groundwater monitoring and sample collection

During a period of 2 years (from January 2013 to December 2014), hydrogeological conditions (groundwater level and salinity), Ra isotopes and ^{222}Rn activities were monitored in the Argentona coastal aquifer using two entirely screened piezometers. The first piezometer, PZ1-, was drilled to a depth of 35 m by the Catalan Water Agency in 2007. It is located 380 m from the shoreline and has a groundwater level approximately 6 - 7 m below the ground surface. The second piezometer, PZ0, which was only monitored for 7 months (May 2014 to December 2014), was drilled approximately 8 m from the shoreline to a depth of 2 m. Three CTD-Diver® data loggers were installed in the piezometers to measure temporal salinity, temperature and groundwater table variations. The first instrument was installed in PZ1 10 m below the ground surface (3 - 4 m below the water level) to evaluate the freshwater conditions (hereinafter referred to as PZ1-S). The second instrument was installed in PZ1 at a depth of 34 m to monitor variations in the mixing zone between the freshwater and saltwater (hereinafter referred to as PZ1-B) (Figure 1). (3) The third instrument was installed in PZ0 at a depth of 1.8 m below the ground surface to evaluate conditions in the groundwater close to the coastal seepage face. Variations in air pressure were compensated for using air pressure measurements that were made simultaneously using a Baro-Diver® that was also installed at the top of the PZ1 piezometer.

Groundwater samples were collected at the same depths where the CTDs were installed, samples from PZ1-S (n=15) were collected 10 m below the ground surface, samples from PZ1-B (n=15)

were collected 34 m below the ground surface, and samples from PZ0 (n=8) were collected 1.5 m below the ground surface). A submersible pump was used to collect samples with volumes of 60 L (PZ1-S), 25 L (PZ1-B) and 10 L (PZ0) for Ra isotopes. Samples with volumes of 250-mL were collected for ^{222}Rn analyses from PZ1-S and PZ1-B. Radon-222 was not analyzed in PZ0 due to the low water level (less than 20 cm), which increased the exchange of ^{222}Rn with the air and did not permit us to obtain a representative sample. During each sampling survey, salinity and temperature were measured *in situ* using a YSI-556 handheld probe.

Water samples for Ra isotopes were filtered through MnO_2-impregnated acrylic fibers (hereinafter referred to as Mn fibers) at flow rates < 1 L min^{-1} to quantitatively sorb Ra onto the Mn fibers (Moore and Reid, 1973). For the ^{222}Rn samples, groundwater was pumped directly through a tube that reached to the bottom of each 250-mL bottle. The groundwater was allowed to overflow for several volumes of the sample bottle to reduce Rn losses to the atmosphere.

2.3 Analytical methods

Once in the laboratory, the Mn fibers containing the Ra isotopes were rinsed with Ra-free water (Sun and Torgersen, 1998), partially dried and placed in a Radium Delayed Coincidence Counter (RaDeCC) to quantify the short-lived Ra isotopes, ^{223}Ra and ^{224}Ra (Garcia-Solsona et al., 2008; Moore and Arnold, 1996). After these measurements, the Mn fibers were ashed (820°C, 16 hours), ground and aged for 3 weeks in counting vials to allow ^{222}Rn to come into secular equilibrium with ^{226}Ra. Samples were measured using a well-type HPGe gamma detector. ^{226}Ra and ^{228}Ra were measured via ^{214}Pb at the 351.9 keV photopeak and ^{228}Ac at the 911 keV photopeak, respectively. ^{222}Rn activities in groundwater samples were determined using a portable ^{222}Rn-in-air alpha spectrometer RAD7 (Durridge Inc.) coupled with a RAD-H_2O attachment that allows the direct determination of ^{222}Rn from 250-mL bottles (Burnett et al., 2001).

3. RESULTS

188 3.1 Hydrogeological features and dynamics

189 Results of the continuous monitoring of the groundwater table and salinity at PZ1 are shown in
190 Figure 2. The fresh groundwater part of the coastal aquifer (PZ1-S) showed relatively constant
191 salinities (~ 0.4) with minimum values of 0.05 occurring during some rainfall events (Figure 2b).
192 In contrast, salinities at the bottom level (PZ1-B) varied significantly during the studied period
193 and ranged from 0.3 to 17 (Figure 2c). Two general patterns in salinity can be identified at the
194 bottom. (1) Salinities were stable during dry periods (sometimes showing minor and constant
195 salinity increases due to reductions in recharge), with maximum values of 15 - 17 (e.g., January –
196 February 2013 and July – September 2013). On the other hand, (2) large fluctuations occur during
197 rainfall events, and sudden decreases in groundwater salinity were followed by gradual increases
198 after rain/recharge episodes. This behavior is exemplified by a particular rainfall event (RFE-8;
199 Figure 2d, 2e). After the precipitation fell, the groundwater table increased by 60 cm and the
200 salinity at the bottom of PZ1 decreased sharply (over 23 hours) from 13 to 0.2. This fast
201 piezometric response to precipitation can be attributed to the hydrogeological features of the
202 alluvial aquifer, which has a high hydraulic conductivity and a small non-saturated zone in the
203 lower part of the basin (Catalan Water Agency, 2010), but it is also accentuated due to the use of a
204 fully screened piezometer (Shalev et al., 2009). Under stable conditions, an equilibrium exists
205 between the aquifer, which is governed by the laws of groundwater motion, and the entire
206 screened piezometer, which is governed by the hydrostatic law (Rushton, 1980). However, under
207 changing conditions, this equilibrium is broken, and the position of the salinity interface in the
208 piezometer may not correspond to its actual position in the aquifer (Rushton, 1980; Tellam et al.,
209 1986; Carrera et al., 2010). For instance, during heavy rainfall events, the higher hydraulic level of
210 fresh groundwater occurring in the upper part of the entirely screened piezometer pushes the
211 saltwater downward faster than it occurs in the aquifer. As a result, after these episodes, salinity
212 decreased faster in the piezometer than in the aquifer itself.

213 Rainfall-derived aquifer recharge produced an increase in the hydraulic gradient between the
214 coastal aquifer and the sea, leading to seaward displacement of the salinity interface and a

215 significant decrease in groundwater salinity in the bottom section of the piezometer (Figure 2c,
216 2e). Once the infiltration of rainfall water had finished, the hydraulic gradient decreased gradually,
217 resulting in landward displacement of the salinity interface and a consequent increase in
218 groundwater salinity in the bottom section of the piezometer (Figure 2c, 2e). While the seaward
219 displacement of the salinity interface occurred shortly (a few hours to days) after the precipitation
220 episode, several weeks or even months were needed to recover the salinity values observed prior
221 to the rain event(s). For instance, salinity at PZ1-B decreased from 13 to 0.3 in less than a day
222 (~23 hours) associated with RFE-8, whereas several months (~6 months) were needed to recover
223 the initial salinity of 13-15 (Figure 2e).

224 Unlike aquifers dominated by tidal cycles, the impact of microtides on the hydraulic gradient, and
225 consequently the position of the salinity interface, can be negligible in PZ1. As shown in Figure
226 2f, the tidal range in the area was on the order of ~20 cm (data compiled from the Barcelona
227 mareograph and obtained from the State Ports Authority; www.puertos.es), a pattern commonly
228 observed in the NW Mediterranean Sea. These small tidal oscillations induced only small
229 variations in the groundwater table and in the groundwater salinities at the bottom of the
230 piezometer (tidally derived groundwater salinity variations of ~1).

231 Regarding PZ0, the piezometer closest to the shoreline but located in the same aquifer unit, the
232 recorded data on groundwater table and salinity followed a similar pattern as those observed in
233 PZ1 (Figure 3). Namely, stable salinities were observed during dry periods, with maximum values
234 of 3 (e.g., May 2014 and August – November 2014), and fluctuations of salinity were observed
235 during rainfall events, with salinity decreasing to reach minimum values of 0.1. Although the
236 piezometers, PZ1 and PZ0, are located 380 and 8 m from the shoreline, respectively, CTDs
237 installed in both piezometers registered almost the same variations in the groundwater table and
238 salinity (e.g., RFE-12, 13, 14 and 16), indicating similar responses to recharge/rain events, as
239 expected. However, various significant increases in groundwater salinities in PZ0 (up to salinities
240 higher than 18) that did not correspond with the fluctuations recorded in PZ1 were also observed.
241 These salinity increases in PZ0 coincided with increases in the significant wave height (H_0) in the
242 coastal sea, mainly related to the eastern storms characteristic of the spring and autumn seasons in

243 the northwestern Mediterranean Sea. The increase in the frequency and height of waves at the
244 shoreline modifies the equilibrium of the hydraulic gradient, moving the salinity interface
245 landward and increasing the salinity in PZ0 (Moore and Wilson, 2005). The influence of these
246 storms on PZ0 lasted for short periods (less than 6 days), and PZ0 rapidly recovered the
247 groundwater salinities observed before storm events, due to the contrary effect of the downward
248 groundwater flow of the aquifer. Given the limited influence of these kind of storm events, the
249 groundwater recharge-discharge cycle appears to be the main driver controlling the position of the
250 salinity interface in the studied NW Mediterranean coastal aquifer.

251 3.2 Ra isotopes and ^{222}Rn characterization in groundwater

252 The activities of Ra isotopes and ^{222}Rn measured in groundwater samples from PZ1-S, PZ1-B and
253 PZ0, together with their corresponding salinities, are presented in Table 1. The activities of Ra
254 isotopes in shallow groundwater (PZ1-S) samples showed relatively constant values that ranged
255 from 0.4 to 3.8 dpm 100 L^{-1} for ^{223}Ra, 40 to 90 dpm 100 L^{-1} for ^{224}Ra, 9 to 20 dpm 100 L^{-1} for
256 ^{226}Ra and 60 to 90 dpm 100 L^{-1} for ^{228}Ra. The activity of Ra in PZ1-B presented a larger
257 variability, and these values ranged from 2 to 80 dpm 100 L^{-1} for ^{223}Ra, 70 to 2100 dpm 100 L^{-1}
258 for ^{224}Ra, 30 to 440 dpm 100 L^{-1} for ^{226}Ra and 70 to 1700 dpm 100 L^{-1} for ^{228}Ra. The activities of
259 Ra isotopes were particularly low during rainfall events, when groundwater salinities in the
260 piezometer were minimal, whereas the largest activities were measured during dry periods that
261 corresponded to the highest groundwater salinities. On the other hand, Ra activities in PZ0
262 showed a similar variability as those seen in PZ1-B, and they ranged from 3 to 10 dpm 100 L^{-1} for
263 ^{223}Ra, 260 to 830 dpm 100 L^{-1} for ^{224}Ra, 40 to 70 dpm 100 L^{-1} for ^{226}Ra and from 200 to 760 dpm
264 100 L^{-1} for ^{228}Ra. Ra activities in groundwater samples were higher than values commonly found
265 in NW Mediterranean coastal aquifers (e.g., Rodellas et al., 2015a), most likely due to the high
266 radium content of the granitic basement (which are rich in ^{232}Th decay chain radionuclides) and
267 the relatively high salinities of the groundwater in the aquifer that favor radium desorption. The
268 activities of Ra isotopes measured in the two piezometers showed strong positive correlations with
269 salinity (R^2=0.91, 0.97, 0.87 and 0.95 for ^{223}Ra, ^{224}Ra, ^{226}Ra and ^{228}Ra, respectively; $p<0.001$),
270 suggesting that the groundwater sampled in PZ0, which is near the discharge area, has similar

characteristics as the groundwater in PZ1 (Figure 4a). Unlike Ra isotopes activities, the activities of ^{222}Rn in groundwater samples reflected relatively constant concentrations in the water samples from PZ1-S and PZ1-B throughout the studied period, with values ranged from $40 \cdot 10^3$ to $120 \cdot 10^3$ dpm 100 L^{-1} (Figure 4b).

A detailed analysis of the rainfall event RFE-8 suggested that Ra activities in groundwater from PZ1-B followed a pattern linked to groundwater recharge cycles (Figure 2; Table 1). Thus, just after the precipitation event, Ra activities diminished by a factor of ~19, ~14, ~6, and ~11 for ^{223}Ra, ^{224}Ra, ^{226}Ra and ^{228}Ra, respectively, in a short period of time (Table 1). A few days after the event, and coupled with an increase of groundwater salinity, Ra activities gradually increased toward the activities measured before the rainfall event. The activity of ^{222}Rn followed a similar pattern to those of the Ra isotopes, although it only decreased by a factor of ~2 (from $81 \cdot 10^3$ to $39 \cdot 10^3$ dpm 100 L^{-1}) after the precipitation event.

4. DISCUSSION

4.1 Variability in the activity of ^{222}Rn and the activities of Ra isotopes

The activities of Ra isotopes measured in groundwater from PZ1 and PZ0 spanned a wide range. In particular, ^{224}Ra in PZ1-B varied by a factor of 31 during the 2 monitored years, whereas ^{222}Rn activities were relatively constant throughout the sampling period and varied by less than a factor of 3. This contrasting pattern between Ra isotopes and ^{222}Rn is likely a consequence of differences in their geochemical behavior in the subterranean estuary. Radium desorption is an exchange process that is highly dependent on the ionic strength (salinity) of the solution; it commonly represents the main factor determining the activities of Ra isotopes dissolved in groundwater (Cho and Kim, 2016; Gonneea et al., 2008). Consequently, the activities of Ra isotopes in fresh groundwater from the shallow depths of the subterranean estuary are considerably lower than those in brackish groundwater from greater depths. Ra activities at the salinity interface are likely explained by binary mixing between low-Ra, low-salinity groundwater and high-Ra, high-salinity groundwater. Indeed, this behavior explains the strong linear correlations between the concentrations of Ra isotopes and groundwater salinities observed over the entire period of the

298 study (Figure 4a). Unlike Ra isotopes, groundwater salinity has little influence on the behavior of
299 ^{222}Rn in the aquifer because it is a noble gas. Moreover, ^{222}Rn supported by ^{226}Ra dissolved in
300 groundwater usually represents a minor fraction of the total ^{222}Rn activity in groundwater.
301 Therefore, similar ^{222}Rn activities are expected in fresh, brackish and salty groundwater, thus
302 explaining the lack of significant correlations between ^{222}Rn activities and salinity in groundwater
303 from the studied site (Figure 4b). However, it should be noted that, after rainfall events, ^{222}Rn
304 activities decreased considerably, together with salinity. This coupled ^{222}Rn-salinity decrease is
305 attributed to dilution that is due to the vertical infiltration of rainwater into the highly permeable
306 coastal aquifer, since rainwater has a salinity close to 0 and contains negligible amounts of ^{222}Rn.
307 After the rainwater had interacted with the geological matrix, the activity of ^{222}Rn in the meteoric
308 fresh water started to increase, due to its production within the aquifer solids. Concentrations in
309 equilibrium with the aquifer matrix were achieved within 15 - 20 days after rainwater infiltration
310 into the aquifer.

311 4.2 Temporal variability of the salinity interface: Implications for Ra- and Rn-derived SGD
312 estimates

313 The position and dynamics of the salinity interface are influenced to a large degree by multiple
314 forcing mechanisms, which include marine (e.g., wave setup and swash infiltration, as well as
315 tidal pumping) and terrestrial drivers (e.g., recharge patterns) (Li et al., 2008; Henderson et al.,
316 2010; Santos et al., 2012; Abarca et al., 2013). Whereas tides are physical forces that are relevant
317 for determining freshwater-seawater mixing in most coastal areas (Kim and Hwang, 2002;
318 Michael et al., 2003; Charette, 2007; Bokuniewicz et al., 2015), they play a minor role in
319 microtidal environments such as the Mediterranean Sea, the Baltic Sea and the Caribbean Sea
320 (Szymczycha et al., 2012; Gonneea et al., 2014; Rodellas et al., 2014;). In such systems, the
321 dynamics of the salinity interface are mainly governed by the inland hydraulic gradient, which
322 mainly reflects the terrestrial groundwater recharge rate (Dausman and Langevin, 2005).
323 Microtidal coastal aquifers are thus highly influenced by precipitation regimes, and they become
324 highly dynamic systems when precipitation events are temporally variable. This pattern is
325 commonly observed in the Mediterranean basin, where 4 - 6 short (lasting hours to a few days)

and intense (a maximum precipitation rate of 40 mm·day^{-1} occurred during the studied period, but it can be much higher) rainfall events represent more than 70% of the annual precipitation (e.g., RFE-1, 8, 13 and 15, Figure 2) (Gasith and Resh, 1999). According to the change in hydraulic gradient observed in PZ0 (the closest to the sea) over a period of nearly 8 months, it can be estimated that 50% of the discharge is produced during and/or within a few days after rain events. Thus, short and intense rainfall events are likely to produce the highest rates of fresh SGD to the coastal sea, which would account for a significant proportion of the freshwater that seeps into the sea yearly. For the rest of the year, fresh SGD flows are expected to be significantly lower and more constant. Thus, estimating SGD fluxes in microtidal systems during periods of intense precipitation are particularly relevant from both a hydrogeological and a biogeochemical perspective.

The quantification of SGD flows to the coastal sea using Ra isotopes and ^{222}Rn requires accurately characterizing their activities in groundwater discharging to the coastal sea (i.e., the SGD end-member). Indeed, Ra- and ^{222}Rn-derived SGD fluxes can only be resolved at levels where the tracer concentration in the end-member is well constrained. Thus, the selection of an appropriate end-member is commonly the main source of uncertainty in final SGD estimates (Cho and Kim, 2016; Burnett et al., 2007; Dulaiova et al., 2008; Garcia-Orellana et al., 2010; Gonneea et al., 2013). Given that Ra isotopes are highly influenced by the ionic strength of the dissolved phase, the process of freshwater-seawater mixing dynamics are key processes in understanding the distribution of Ra in a coastal aquifer and constraining the Ra concentration in the SGD end-member (Charette et al., 2001; Gonneea et al., 2013; Michael et al., 2011). Indeed, several studies have reported that the activities of Ra isotopes in the SGD end-member vary over a wide range (up to orders of magnitude) both in space and time, and are often linked to changes in the ionic strength of the dissolved phase (Cho and Kim, 2016). Thus, accurately evaluating the complex and dynamic mixing of fresh groundwater with seawater (i.e., the position of the salinity interface) becomes critical for obtaining reliable Ra-derived SGD estimates.

In highly dynamic microtidal systems, achieving an appropriate understanding of the hydrodynamics of coastal aquifers requires significant monitoring and characterization efforts that

354 are often unavailable when SGD studies are conducted. To overcome this limited hydrogeological
355 understanding, studies that use Ra isotopes to quantify SGD commonly rely on collecting a
356 relatively large number of samples, as well as using different approaches to characterize the SGD
357 end-member (potential approaches include, e.g., averaging the Ra activities from all the samples
358 collected (Gonneea et al., 2014), taking the maximum measured Ra activities to obtain
359 conservative estimates (Moore, 1996b), or using ranges of Ra activities covering the samples
360 collected (Kim et al., 2005). Whereas these approaches may work in many of the tidal systems
361 studied, using them in coastal aquifers characterized by highly dynamic freshwater-seawater
362 mixing zones (with large salinity and thus large Ra variations) may introduce large uncertainties
363 into the final SGD quantification. Constraining Ra activities in the SGD end-member during (or
364 just after) intense rainfall events may be particularly challenging, given the large temporal
365 variations in salinity and Ra in coastal groundwater, making it difficult to obtain reliable SGD
366 estimates. As detailed above, it should be noted that inputs of fresh groundwater to coastal seas are
367 expected to be much higher during these rainfall periods, and thus, the SGD evaluations during
368 these periods have a major hydrological and biogeochemical interest. Conversely, Ra activities in
369 the SGD end-member can be more easily constrained during dry periods because they are
370 associated with reduced variability in coastal groundwater, thus allowing appropriate estimates of
371 Ra-derived SGD fluxes to be made for the rest of the year.

372 Unlike Ra isotopes, the activity of ^{222}Rn in coastal groundwater appears to be relatively constant
373 throughout the year due to the relatively small influence of groundwater salinity on ^{222}Rn
374 behavior, even during intense rainy events (^{222}Rn activities only varied by a factor 2 during these
375 events). These small variations allow us to better constraint the activity of ^{222}Rn in the SGD end-
376 member and, thus, better estimate SGD flows during rainy periods. This observed pattern suggests
377 that ^{222}Rn may be a more appropriate SGD tracer than Ra isotopes in systems with highly dynamic
378 salinity interfaces, particularly during the wet season, when groundwater salinities (and thus Ra
379 activities) may change significantly over short temporal scales. However, whereas the Rn end-
380 member can be relatively well constrained, Rn-derived SGD estimates are highly sensitive to Rn
381 mixing losses and especially the loss of Rn to the atmosphere by degassing. These two loss terms

are difficult to determine, particularly under conditions with strong winds and high waves, which often occur concurrently with eastern storm events.

5. CONCLUSIONS

Understanding the behavior of tracers used to determine submarine groundwater discharge (SGD) fluxes is crucial for accurately quantifying groundwater- and chemical- driven fluxes to the ocean in order to better understand coastal biogeochemical cycles. The results obtained in this work reveal that activities of Ra isotopes, which are commonly used tracers to quantify SGD, show a large variability in microtidal coastal groundwater systems throughout the year and particularly during intense rainfall events (e.g., activity changes by a factor of ~19, ~14, ~6, and ~11 for ^{223}Ra, ^{224}Ra, ^{226}Ra and ^{228}Ra during a particular rainfall event, RFE-8). This large variability, which is linked to the displacement of the salinity interface seawards, complicates the accurate estimation of the Ra-SGD end-member, resulting in Ra-derived SGD estimates with large uncertainties. In contrast, ^{222}Rn activities present only minor variations (by a factor of 3), as a consequence of the relatively small influence of groundwater salinity on ^{222}Rn activities. In microtidal systems, high SGD-driven fluxes to the sea of both freshwater and dissolved chemical compounds are expected to occur during the rainy season and/or intense rainfall events. Thus, scientific efforts should be particularly directed toward understanding SGD fluxes during this season, when the influence of SGD on hydrological budgets is expected to be significant. The observed differences between the rainy season and the dry period indicate that appropriate SGD quantification over longer (monthly or yearly) time scales cannot be carried out properly without considering the temporal variability in Ra activities.

In addition to the difficulties in estimating SGD flows during rainfall events (which are mainly due to the difficulty of characterizing the SGD end-member), the extreme variability in the concentrations of chemical compounds (e.g., nutrients, trace metals, contaminants, and other species) in the groundwater poses an additional challenge in constraining a representative groundwater end-member. The fluxes of dissolved compounds transported by SGD have usually been calculated by multiplying the SGD flux derived using Ra isotopes or Rn by the concentration

410 of the chemical compounds in the inflowing SGD. As in the case of the Ra end-member, it is
411 particularly critical to identify a representative concentration of the studied dissolved chemical
412 compound in the discharging groundwater during intense rainfall events. A poor understanding of
413 the behavior of dissolved chemicals in the coastal aquifer during rainfall events may lead to large
414 uncertainties in SGD-driven chemical fluxes. Since the SGD-driven fluxes during the wet periods
415 may account for a significant fraction of the chemical fluxes to the coastal areas, it is expected that
416 the impact of SGD on coastal biogeochemical cycles is particularly relevant during these events.
417 Characterizing the behavior of Ra/Rn and dissolved chemical compounds within subterranean
418 estuaries during rainfall events in microtidal systems remains a challenge, which must be
419 considered in future studies of SGD-driven nutrient fluxes to coastal areas in order to understand
420 the relative impact of SGD on coastal biogeochemical cycles.

421

422 ACKNOWLEDGMENTS

423 This work was funded by projects CGL2013-48869-C2-1 and CGL2013-48869-C2-2-R of the
424 Spanish Government. M.C.D acknowledges financial support from the Ministerio de Economía y
425 Competitividad (PhD fellowship, A-2014-9185) through the NUREIEV project (CTM2013-
426 44598-R) coordinated by GRC Geociències Marines of the Departament de Dinàmica de la Terra i
427 de l'Oceà (Universitat de Barcelona). The authors wish to thank the Generalitat de Catalunya for
428 its support of MERS (2014 SGR-1356) and Agència Catalana de l'Aigua (ACA). V.R. also
429 acknowledges financial support from the European Union's FP7 program (Marie Curie Actions
430 PCOFUND-GA-2013-609102) through the PRESTIGE program coordinated by Campus France.
431 This study is a contribution to the ANR @RAction chair (ANR-14-ACHN-0007-01) and Labex
432 OT-Med (ANR-11-LABEX-0061), which was funded by the "Investissements d'Avenir" program
433 through the A*MIDEX project (ANR-11-IDEX-0001-02) of the French National Research
434 Agency (ANR).

435

436 GRAPHICAL ABSTRACT

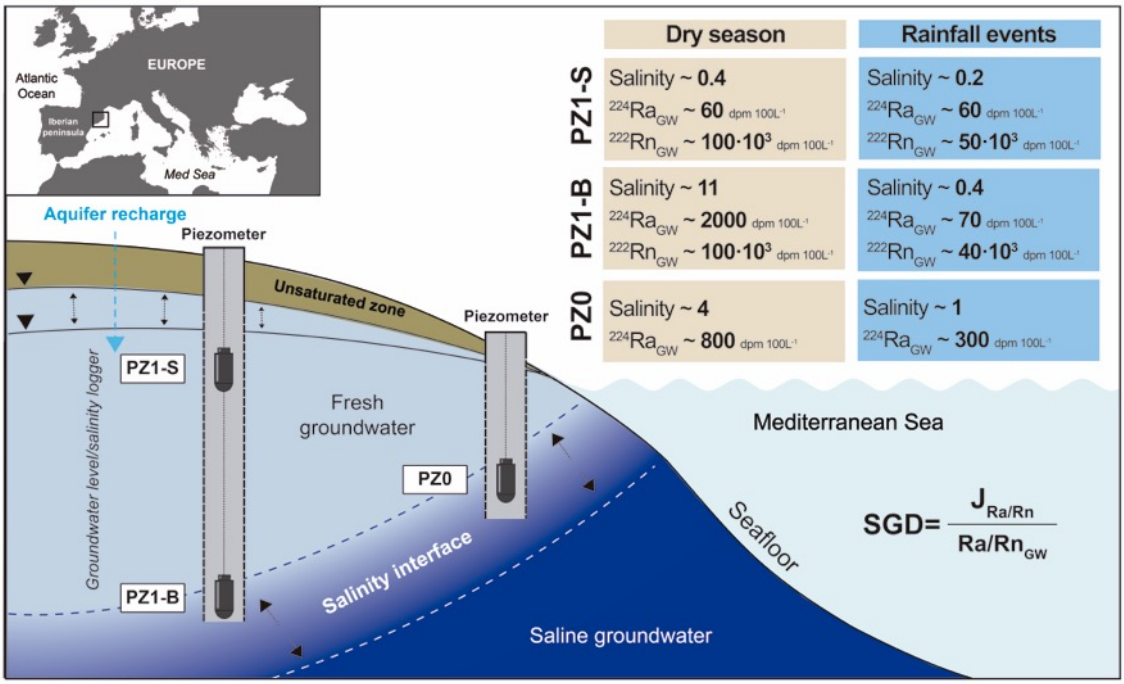

437

438

439

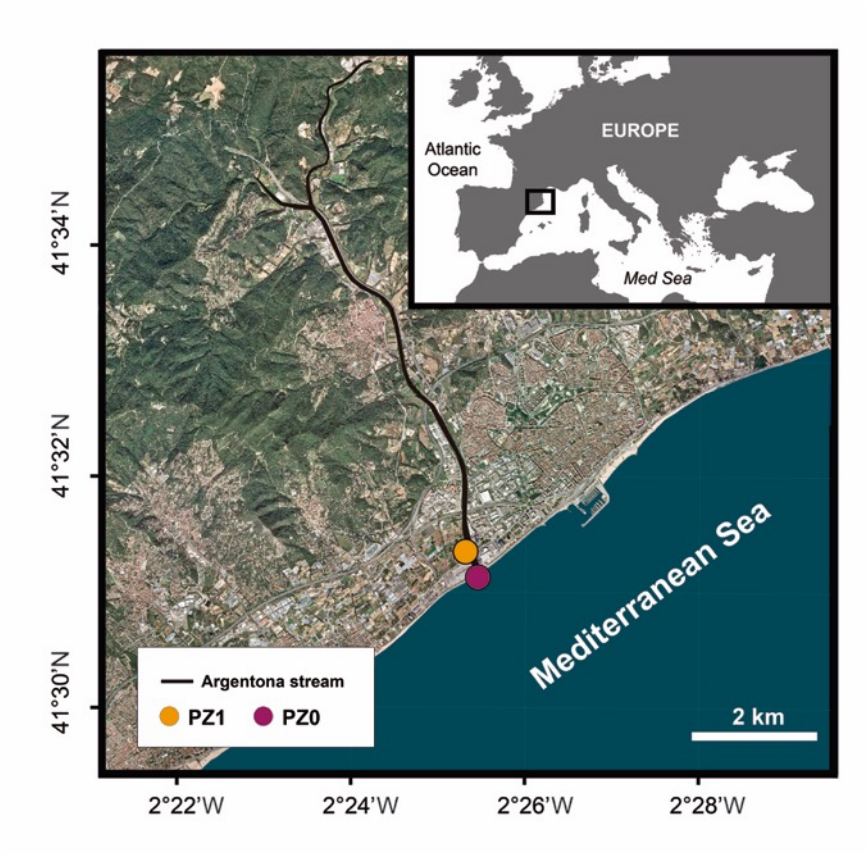

440

441 **Figure 1**. Location of the Argentona stream in the NW Mediterranean Sea, including the location

442 of the two monitored piezometers (PZ).

443

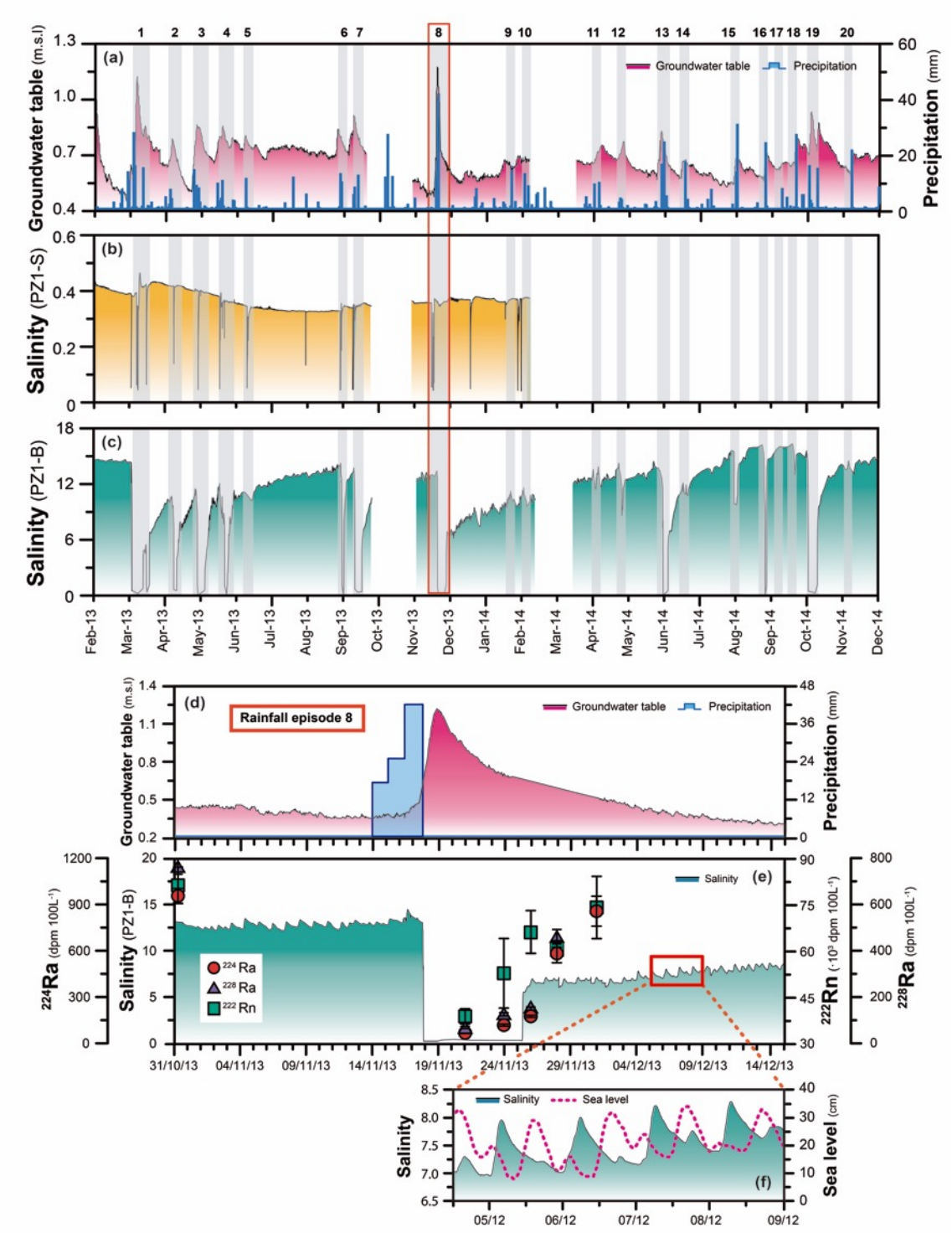

Figure 2. Temporal evolution of the hydrogeological conditions and the Ra and Rn activities in the coastal aquifer: (a) Daily cumulative precipitation in the area and measured groundwater table elevations in the coastal aquifer; (b) and (c) groundwater salinities in the shallow (PZ1-S) and bottom (PZ1-B) parts, respectively, of piezometer PZ1; (d) groundwater table elevation and precipitation records from rainfall episode 8 (RFE-8); (e) Variations in Rn and Ra activities and salinity in PZ1-B

during RFE-8; (f) Sea level and salinity oscillations in PZ1-B. Vertical gray lines indicate rainfall events (RFEs) that significantly affected groundwater table elevation.

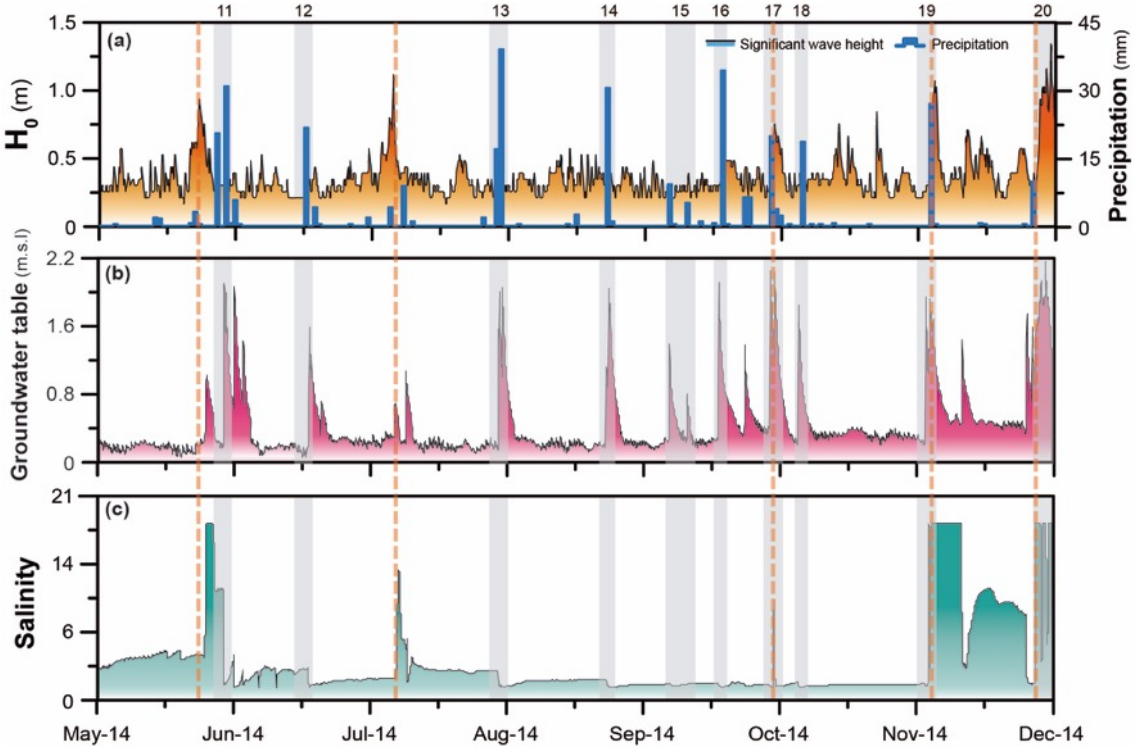

Figure 3. Temporal evolution of hydrogeological conditions in PZ0: (a) Significant wave heights of coastal seawater (H_0) derived from the SIMAR dataset (2115138) oceanographic model (State Ports Authority; www.puertos.es); (b) daily cumulative precipitation in the area and measured groundwater table elevations in the coastal aquifer; (c) groundwater salinities in PZ0. Vertical gray lines and orange dotted lines indicate the major rainfall events (RFEs) and eastern storm events, respectively, that significantly affected groundwater table elevation or salinity in PZ0.

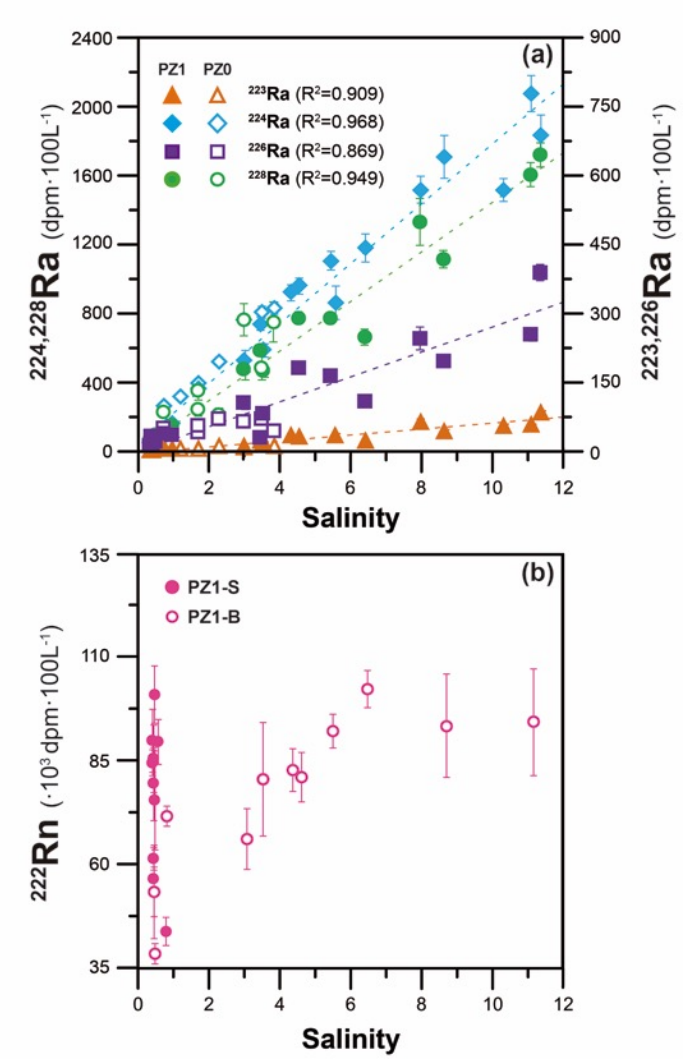

Figure 4. Ra isotopes and ^{222}Rn activities vs salinity in groundwater from the Argentona aquifer (PZ1-S, PZ1-B and PZ0). Dashed lines represent the best linear fits to the data.

	Date	Sal	^{222}Rn	^{223}Ra	^{224}Ra	^{226}Ra	^{228}Ra	^{224}Ra/^{228}Ra AR	^{226}Ra/^{228}Ra AR
			(10^3 dpm 100L^{-1})		(dpm 100 L^{-1})				
PZ1-S (shallow)									
ARG3-PZ1-S	20/12/12	0.51	90 ± 5	2.0 ± 0.3	85 ± 5	18 ± 1	85 ± 4	0.99 ± 0.08	0.21 ± 0.01
ARG4-PZ1-S	29/1/13	0.42	101 ± 7	0.8 ± 0.2	53 ± 3	9 ± 1	70 ± 3	0.76 ± 0.04	0.13 ± 0.02
ARG6-PZ1-S	24/4/13	0.39	86 ± 8	0.8 ± 0.2	56 ± 4	14 ± 1	65 ± 4	0.87 ± 0.08	0.22 ± 0.02
ARG7-PZ1-S	28/5/13	0.36	90 ± 8	0.9 ± 0.1	50 ± 3	10 ± 1	56 ± 1	0.90 ± 0.05	0.18 ± 0.02
ARG8-PZ1-S	28/6/13	0.35	85 ± 3	0.4 ± 0.2	44 ± 3	n.a	n.a	n.a	n.a
ARG10-PZ1-S	23/9/13	0.39	80 ± 9	1.5 ± 0.2	66 ± 3	n.a	n.a	n.a	n.a
ARG11-PZ1-S	30/10/13	0.40	76 ± 12	1.2 ± 0.2	68 ± 3	13 ± 1	65 ± 5	1.05 ± 0.10	0.20 ± 0.02
ARG12-PZ1-S	21/11/13	0.37	45 ± 3	0.8 ± 0.2	59 ± 3	12 ± 1	62 ± 5	0.95 ± 0.09	0.19 ± 0.02
ARG13-PZ1-S	24/11/13	0.37	57 ± 6	0.9 ± 0.2	56 ± 3	n.a	n.a	n.a	n.a
ARG15-PZ1-S	26/11/13	0.39	62 ± 3	0.6 ± 0.2	61 ± 3	n.a	n.a	n.a	n.a
ARG16-PZ1-S	28/11/13	0.39	57 ± 8	0.5 ± 0.2	60 ± 3	13 ± 1	68 ± 5	0.88 ± 0.08	0.19 ± 0.02
ARG17-PZ1-S	1/12/13	0.39	52 ± 4	0.8 ± 0.2	59 ± 3	n.a	n.a	n.a	n.a
ARG18-PZ1-S	9/12/13	0.38	n.a	0.4 ± 0.2	56 ± 3	n.a	n.a	n.a	n.a
ARG19-PZ1-S	9/2/14	0.36	n.a	0.5 ± 0.2	43 ± 2	n.a	n.a	n.a	n.a
ARG20-PZ1-S	13/4/14	0.39	n.a	3.8 ± 0.5	62 ± 3	12 ± 1	60 ± 5	1.04 ± 0.10	0.20 ± 0.02
PZ1-B (bottom)									
ARG3-PZ1-B	20/12/12	8.68	94 ± 12	42 ± 5	1704 ± 123	193 ± 11	1108 ± 50	1.54 ± 0.13	0.17 ± 0.01
ARG4-PZ1-B	29/1/13	6.43	103 ± 5	21 ± 2	1179 ± 90	106 ± 8	658 ± 47	1.79 ± 0.18	0.16 ± 0.02
ARG6-PZ1-B	24/4/13	11.14	95 ± 13	55 ± 4	2074 ± 108	251 ± 11	1596 ± 68	1.30 ± 0.09	0.16 ± 0.01
ARG7-PZ1-B	28/5/13	3.47	81 ± 14	20 ± 2	737 ± 40	26 ± 2	574 ± 27	1.28 ± 0.09	0.05 ± 0.01
ARG8-PZ1-B	28/6/13	5.46	92 ± 4	22 ± 1	1102 ± 50	161 ± 7	762 ± 30	1.45 ± 0.09	0.21 ± 0.01
ARG10-PZ1-B	23/9/13	4.32	83 ± 5	33 ± 2	917 ± 50	n.a	n.a	n.a	n.a
ARG11-PZ1-B	30/10/13	4.55	81 ± 6	30 ± 2	956 ± 50	178 ± 8	764 ± 30	1.25 ± 0.08	0.23 ± 0.01
ARG12-PZ1-B	21/11/13	0.39	39 ± 2	1.6 ± 0.5	67 ± 4	29 ± 6	68 ± 5	0.99 ± 0.08	0.42 ± 0.09
ARG13-PZ1-B	24/11/13	0.74	53 ± 11	3.6 ± 0.5	118 ± 7	34 ± 2	125 ± 7	0.94 ± 0.08	0.28 ± 0.02
ARG15-PZ1-B	26/11/13	0.98	66 ± 7	3 ± 1	160 ± 8	33 ± 2	139 ± 7	1.15 ± 0.08	0.24 ± 0.02
ARG16-PZ1-B	28/11/13	3.57	61 ± 2	17 ± 2	582 ± 40	79 ± 6	461 ± 30	1.26 ± 0.12	0.17 ± 0.02
ARG17-PZ1-B	1/12/13	5.60	74 ± 10	33 ± 4	856 ± 100	n.a	n.a	n.a	n.a
ARG18-PZ1-B	9/12/13	8.00	82 ± 5	61 ± 7	1516 ± 80	244 ± 30	1344 ± 137	1.14 ± 0.13	0.18 ± 0.03
ARG19-PZ1-B	9/2/14	10.36	n.a	23 ± 2	1513 ± 70	n.a	n.a	n.a	n.a
ARG20-PZ1-B	13/4/14	11.42	n.a	82 ± 6	1834 ± 121	440 ± 18	1715 ± 70	1.07 ± 0.08	0.22 ± 0.01
PZ0									
ARG21-PZ0	24/4/14	0.75	n.a	5 ± 0.4	257 ± 11	47 ± 4	222 ± 12	1.16 ± 0.08	0.21 ± 0.02
ARG22-PZ0	30/4/14	2.99	n.a	9 ± 2	762 ± 33	62 ± 7	755 ± 95	1.01 ± 0.13	0.08 ± 0.01
ARG23-PZ0	13/5/14	3.85	n.a	9 ± 2	828 ± 35	40 ± 7	741 ± 117	1.12 ± 0.18	0.05 ± 0.01
ARG24-PZ0	16/5/14	3.51	n.a	12 ± 2	802 ± 37	67 ± 4	480 ± 67	1.67 ± 0.25	0.14 ± 0.02
ARG25-PZ0	3/6/14	1.20	n.a	3 ± 1	313 ± 15	n.a	n.a	n.a	n.a

ARG26-PZ0	7/6/14	1.70	n.a	4 ± 1	392 ± 19	38 ± 6	232 ± 34	1.69 ± 0.26	0.16 ± 0.04	476
ARG27-PZ0	11/6/14	1.70	n.a	4 ± 1	357 ± 16	55 ± 11	343 ± 51	1.04 ± 0.16	0.16 ± 0.04	
ARG28-PZ0	26/6/14	2.30	n.a	8 ± 2	517 ± 23	67 ± 12	200 ± 44	2.59 ± 0.58	0.34 ± 0.10	477

n.a: not analyzed

478

479 **Table 1**. Salinity, Ra isotopes and ^{222}Rn activities and Activity Ratios (ARs) in the shallow and bottom parts of piezometer PZ1 (n.a: not analyzed).

480
481 REFERENCES

482 Abarca, E., Karam, H., Hemond, H.F., Harvey, C.F., 2013. Transient groundwater dynamics in a coastal
483 aquifer: The effects of tides, the lunar cycle, and the beach profile. Water Resour. Res. 49, 2473–2488.
484 doi:10.1002/wrcr.20075
485 Beck, A.J., Cochran, M.A., 2013. Controls on solid-solution partitioning of radium in saturated marine sands
486 Mar. Chem. 156, 38–48. doi:10.1016/j.marchem.2013.01.008
487 Beck, A.J., Rapaglia, J.P., Cochran, J.K., Bokuniewicz, H.J., Yang, S., 2008. Submarine groundwater
488 discharge to Great South Bay, NY, estimated using Ra isotopes. Mar. Chem. 109, 279–291.
489 doi:10.1016/j.marchem.2007.07.011
490 Bokuniewicz, H., Cochran, J.K., Garcia-Orellana, J., Rodellas, V., Daniel, J.W., Heilbrun, C., 2015. Intertida
491 percolation through beach sands as a source of 224,223 Ra to Long Island Sound, New York, and
492 Connecticut, United States. J. Mar. Res. 73, 123–140.
493 Burnett, W.C., Bokuniewicz, H., Huettel, M., Moore, W., Taniguchi, M., 2003. Groundwater and pore water
494 inpunts to the coastal zone. Biogeochemistry 66, 3–33.
495 Burnett, W.C., Dulaiova, H., 2003. Estimating the dynamics of groundwater input into the coastal zone via
496 continuous radon-222 measurements. J. Environ. Radioact. 69, 21–35. doi:10.1016/S0265-
497 931X(03)00084-5
498 Burnett, W.C., Peterson, R., Moore, W.S., de Oliveira, J., 2008. Radon and radium isotopes as tracers of
499 submarine groundwater discharge – Results from the Ubatuba, Brazil SGD assessment intercomparison.
500 Estuar. Coast. Shelf Sci. 76, 501–511. doi:10.1016/j.ecss.2007.07.027
501 Burnett, W.C., Taniguchi, M., Oberdorfer, J., 2001. Measurement and significance of the direct discharge of
502 groundwater into the coastal zone. J. Sea Res. 46, 109–116. doi:10.1016/S1385-1101(01)00075-2
503 Burnett, W.C., Wattayakorn, G., Taniguchi, M., Dulaiova, H., Sojisuporn, P., Rungsupa, S., Ishitobi, T., 200
504 Groundwater-derived nutrient inputs to the Upper Gulf of Thailand. Cont. Shelf Res. 27, 176–190.
505 doi:10.1016/j.csr.2006.09.006
506 Burnett, W.C.C., Aggarwal, P.K.K., Aureli, A., Bokuniewicz, H., Cable, J.E.E., Charette, M.A. a, Kontar, E.
507 Krupa, S., Kulkarni, K.M.M., Loveless, A., Moore, W.S.S., Oberdorfer, J.A. a, Oliveira, J., Ozyurt, N.,
508 Povinec, P., Privitera, A.M.G.M.G., Rajar, R., Ramessur, R.T.T., Scholten, J., Stieglitz, T., Taniguchi,
509 M., Turner, J.V. V, 2006. Quantifying submarine groundwater discharge in the coastal zone via multiple
510 methods. Sci. Total Environ. 367, 498–543. doi:10.1016/j.scitotenv.2006.05.009
511 Carrera, J., Hidalgo, J.J., Slooten, L.J., Vazquez-Sune, E., 2010. Computational and conceptual issues in the
512 calibration of seawater intrusion models. Hydrogeol. J. 18, 131–145. doi:10.1007/s10040-009-0524-1
513 Catalan Water Agency, 2010. Model numèric de l'aqüífer al·luvial de la riera d'argentona.
514 Charette, M.A., 2007. Hydrologic forcing of submarine groundwater discharge: Insight from a seasonal study
515 of radium isotopes in a groundwater-dominated salt marsh estuary. Limnol. Oceanogr. 52, 230–239.
516 doi:10.4319/lo.2007.52.1.0230
517 Charette, M. a., Buesseler, K.O., Andrews, J.E., 2001. Utility of radium isotopes for evaluating the input and
518 transport of groundwater-derived nitrogen to a Cape Cod estuary. Limnol. Oceanogr. 46, 465–470.
519 doi:10.4319/lo.2001.46.2.0465
520 Cho, H.-M., Kim, G., 2016. Determining groundwater Ra end-member values for the estimation of the
521 magnitude of submarine groundwater discharge using Ra isotope tracers. Geophys. Res. Lett. 43, 3865–
522 3871. doi:10.1002/2016GL068805
523 Dausman, A., Langevin, C.D., 2005. Movement of the saltwater interface in the surficial aquifer system in
524 response to hydrologic stresses and water-management practices, Broward County, Florida.
525 Dulaiova, H., Gonneea, M.E., Henderson, P.B., Charette, M. a., 2008. Geochemical and physical sources of
526 radon variation in a subterranean estuary - Implications for groundwater radon activities in submarine
527 groundwater discharge studies. Mar. Chem. 110, 120–127. doi:10.1016/j.marchem.2008.02.011
528 Elsinger, R.J., Moore, W.S., 1980. 226Ra behavior in the Pee Dee River-Winyah Bay estuary. Earth Planet.
529 Sci. Lett. 48, 239–249. doi:10.1016/0012-821X(80)90187-9
530 Garcia-Orellana, J., Cochran, J.K., Bokuniewicz, H., Yang, S., Beck, a J., 2010. Time-series sampling of

223Ra and 224Ra at the inlet to Great South Bay (New York): A strategy for characterizing the dominar terms in the Ra budget of the bay. J. Environ. Radioact. 101, 582–588. doi:10.1016/j.jenvrad.2009.12.0(
Garcia-Solsona, E., Garcia-Orellana, J., Masqué, P., Dulaiova, H., 2008. Uncertainties associated with 223Ra and 224Ra measurements in water via a Delayed Coincidence Counter (RaDeCC). Mar. Chem. 109, 198 219. doi:10.1016/j.marchem.2007.11.006
Gasith, A., Resh, V.H., 1999. STREAMS IN MEDITERRANEAN CLIMATE REGIONS: Abiotic Influence and Biotic Responses to Predictable Seasonal Events. Annu. Rev. Ecol. Syst. 30, 51–81. doi:10.1146/annurev.ecolsys.30.1.51
Gonneea, M.E., Charette, M.A., Liu, Q., Herrera-Silveira, J.A., Morales-Ojeda, S.M., 2014. Trace element geochemistry of groundwater in a karst subterranean estuary (Yucatan Peninsula, Mexico). Geochim. Cosmochim. Acta 132, 31–49. doi:10.1016/j.gca.2014.01.037
Gonneea, M.E., Morris, P.J., Dulaiova, H., Charette, M. a., 2008. New perspectives on radium behavior with a subterranean estuary. Mar. Chem. 109, 250–267. doi:10.1016/j.marchem.2007.12.002
Gonneea, M.E., Mulligan, A.E., Charette, M.A., 2013. Seasonal cycles in radium and barium within a subterranean estuary: Implications for groundwater derived chemical fluxes to surface waters. Geochim. Cosmochim. Acta 119, 164–177. doi:10.1016/j.gca.2013.05.034
Heiss, J.W., Michael, H.A., 2014. Saltwater-freshwater mixing dynamics in a sandy beach aquifer over tidal, spring-neap, and seasonal cycles. Water Resour. Res. 50. doi:10.1002/2014WR015574
Henderson, R.D., Day-Lewis, F.D., Abarca, E., Harvey, C.F., Karam, H.N., Liu, L., Lane, J.W.J., 2010. Marine electrical resistivity imaging of submarine groundwater discharge: sensitivity analysis and application in Waquoit Bay, Massachusetts, USA. Hydrogeol. J. 18, 173–185. doi:10.1007/s10040-009-0498-z
Johnson, A.G., Glenn, C.R., Burnett, W.C., Peterson, R.N., Lucey, P.G., 2008. Aerial infrared imaging revea large nutrient-rich groundwater inputs to the ocean. Geophys. Res. Lett. 35, L15606. doi:10.1029/2008GL034574
Kim, G., Hwang, D.-W., 2002. Tidal pumping of groundwater into the coastal ocean revealed from submarin 222 Rn and CH 4 monitoring. Geophys. Res. Lett. 29, 23-1-23–4. doi:10.1029/2002GL015093
Kim, G., Lee, K.-K., Park, K.-S., Hwang, D.-W., Yang, Han-Soeb, Y., 2003. Large submarine groundwater discharge (SGD) from a volcanic island. Geophys. Res. Lett. 30, 2098. doi:10.1029/2003GL018378
Kim, G., Yun, S.-T., Yang, H.-S., Ryu, J.-W., Burnett, W.C., Dulaiova, H., Sholkovitz, E., Moore, W.S., Charette, M. a., Bokuniewicz, H.J., Chanton, J.P., Yun, S.-T., Yang, H.-S., Ryu, J.-W., 2005. Submarine groundwater discharge (SGD) into the Yellow Sea revealed by 228Ra and 226Ra isotopes: Implications for global silicate fluxes. Earth Planet. Sci. Lett. 237, 156–166. doi:10.1016/j.epsl.2005.06.011
Lee, C.M., Jiao, J.J., Luo, X., Moore, W.S., 2012. Estimation of submarine groundwater discharge and associated nutrient fluxes in Tolo Harbour, Hong Kong. Sci. Total Environ. 433, 427–433. doi:10.1016/j.scitotenv.2012.06.073
Li, H., Boufadel, M.C., Weaver, J.W., 2008. Tide-induced seawater-groundwater circulation in shallow beac aquifers. J. Hydrol. 352, 211–224. doi:10.1016/j.jhydrol.2008.01.013
Michael, H.A., Charette, M.A., Harvey, C.F., 2011. Patterns and variability of groundwater flow and radium activity at the coast: A case study from Waquoit Bay, Massachusetts. Mar. Chem. 127, 100–114. doi:10.1016/j.marchem.2011.08.001
Michael, H.A., Lubetsky, J.S., Harvey, C.F., 2003. Characterizing submarine groundwater discharge: A seepage meter study in Waquoit Bay, Massachusetts. Geophys. Res. Lett. 30. doi:10.1029/2002GL0160
Montoto, M., 1967. Estudio petrológico y petrogenético de las rocas graníticas de la Cadena Litoral Catalana 800.
Moore, W.S., 2003. Sources and fluxes of submarine groundwater discharge delineated by radium isotopes. Biogeochemistry 66, 75–93. doi:10.1023/B:BIOG.0000006065.77764.a0
Moore, W.S., 1999. The subterranean estuary: a reaction zone of ground water and sea water. Mar. Chem. 65 111–125.
Moore, W.S., 1996a. Using the radium quartet for evaluating groundwater input and water exchange in salt marshes. Geochim. Cosmochim. Acta 60, 4645–4652. doi:10.1016/S0016-7037(96)00289-X

582 Moore, W.S., 1996b. Large groundwater inputs to coastal waters revealed by 226Ra enrichments. Nature 380
583 612–614. doi:10.1038/380612a0
584 Moore, W.S., Arnold, R., 1996. Measurement of 223Ra and 224Ra in coastal waters using a delayed
585 coincidence counter. J. Geophys. Res. 101, 1321–1329. doi:10.1029/95jc03139
586 Moore, W.S., Reid, D.F., 1973. Extraction of radium from natural waters using manganese-impregnated
587 acrylic fibers. J. Geophys. Res. 78, 8880. doi:10.1029/JC078i036p08880
588 Moore, W.S., Wilson, A.M., 2005. Advective flow through the upper continental shelf driven by storms,
589 buoyancy, and submarine groundwater discharge. Earth Planet. Sci. Lett. 235, 564–576.
590 doi:10.1016/j.epsl.2005.04.043
591 Ollivier, P., Claude, C., Radakovitch, O., Hamelin, B., 2007. TIMS measurements of 226Ra and 228Ra in the
592 Gulf of Lion, an attempt to quantify submarine groundwater discharge. Mar. Chem. 109, 337–354.
593 doi:10.1016/j.marchem.2007.08.006
594 Pavlidou, A., Papadopoulos, V.P., Hatzianestis, I., Simboura, N., Patiris, D., Tsabaris, C., 2014. Chemical
595 inputs from a karstic submarine groundwater discharge (SGD) into an oligotrophic Mediterranean coasta
596 area. Sci. Total Environ. 488, 1–13. doi:10.1016/j.scitotenv.2014.04.056
597 Rodellas, V., Garcia-Orellana, J., Masqué, P., Feldman, M., Weinstein, Y., 2015a. Submarine groundwater
598 discharge as a major source of nutrients to the Mediterranean Sea. Proc. Natl. Acad. Sci. 112, 20141904
599 doi:10.1073/pnas.1419049112
600 Rodellas, V., Garcia-Orellana, J., Masqué, P., Font-Muñoz, J.S., 2015b. The influence of sediment sources on
601 radium-derived estimates of Submarine Groundwater Discharge. Mar. Chem. 171, 107–117.
602 doi:10.1016/j.marchem.2015.02.010
603 Rodellas, V., Garcia-Orellana, J., Tovar-Sánchez, A., Basterretxea, G., López-Garcia, J.M., Sánchez-Quiles,
604 D., Garcia-Solsona, E., Masqué, P., 2014. Submarine groundwater discharge as a source of nutrients and
605 trace metals in a Mediterranean bay (Palma Beach, Balearic Islands). Mar. Chem. 160, 56–66.
606 doi:10.1016/j.marchem.2014.01.007
607 Rodellas, V., Garcia-Orellana, J., Trezzi, G., Masqué, P., Stieglitz, T.C., Bokuniewicz, H., Cochran, J.K.,
608 Berdalet, E., 2017. Using the radium quartet to quantify submarine groundwater discharge and porewate
609 exchange. Geochim. Cosmochim. Acta 196, 58–73. doi:http://dx.doi.org/10.1016/j.gca.2016.09.016
610 Rushton, K.R., 1980. Differing positions of saline interfaces in aquifers and observation boreholes. J. Hydrol
611 48, 185–189. doi:10.1016/0022-1694(80)90074-8
612 Sadat-Noori, M., Santos, I.R., Tait, D.R., Maher, D.T., 2016. Fresh meteoric versus recirculated saline
613 groundwater nutrient inputs into a subtropical estuary. Sci. Total Environ. 566, 1440–1453.
614 doi:10.1016/j.scitotenv.2016.06.008
615 Santos, I.R., Eyre, B.D., Huettel, M., 2012. The driving forces of porewater and groundwater flow in
616 permeable coastal sediments: A review. Estuar. Coast. Shelf Sci. 98, 1–15.
617 doi:10.1016/j.ecss.2011.10.024
618 Shalev, E., Lazar, A., Wollman, S., Kington, S., Yechieli, Y., Gvirtzman, H., 2009. Biased monitoring of fres
619 water-salt water mixing zone in coastal aquifers. Ground Water 47, 49–56. doi:10.1111/j.1745-
620 6584.2008.00502.x
621 Smoak, J.M., Sanders, C.J., Patchineelam, S.R., Moore, W.S., 2012. Radium mass balance and submarine
622 groundwater discharge in Sepetiba Bay, Rio de Janeiro State, Brazil. J. South Am. Earth Sci. 39, 44–51.
623 doi:10.1016/j.jsames.2012.07.004
624 Sun, Y., Torgersen, T., 1998. The effects of water content and Mn-fiber surface conditions on 224Ra
625 measurement by 220Rn emanation. Mar. Chem. 62, 299–306. doi:10.1016/S0304-4203(98)00019-X
626 Swarzenski, P.W., 2007. U/Th Series Radionuclides as Coastal Groundwater Tracers. Chem. Rev. 107, 663–
627 674. doi:10.1021/cr0503761
628 Szymczycha, B., Vogler, S., Pempkowiak, J., 2012. Nutrient fluxes via submarine groundwater discharge to
629 the Bay of Puck, southern Baltic Sea. Sci. Total Environ. 438, 86–93. doi:10.1016/j.scitotenv.2012.08.0
630 Tellam, J.H., Lloyd, J.W., Walters, M., 1986. The morphology of a saline groundwater body: Its investigation
631 description and possible explanation. J. Hydrol. 83, 1–21. doi:10.1016/0022-1694(86)90179-4
632 Tovar-Sánchez, A., Basterretxea, G., Rodellas, V., Sánchez-Quiles, D., García-Orellana, J., Masqué, P., Jordi

633 A., López, J.M., Garcia-Solsona, E., 2014. Contribution of Groundwater Discharge to the Coastal
634 Dissolved Nutrients and Trace Metal Concentrations in Majorca Island: Karstic vs Detrital Systems.
635 Environ. Sci. Technol. 48, 11819–11827. doi:10.1021/es502958t
636 Trezzi, G., Garcia-Orellana, J., Rodellas, V., Santos-Echeandia, J., Tovar-Sánchez, A., Garcia-Solsona, E.,
637 Masqué, P., 2016. Submarine groundwater discharge: A significant source of dissolved trace metals to t
638 North Western Mediterranean Sea. Mar. Chem. 186, 90–100. doi:10.1016/j.marchem.2016.08.004
639 Webster, I.T., Hancock, G.J., Murray, A.S., 1995. Modelling the effect of salinity on radium desorption from
640 sediments. Geochim. Cosmochim. Acta 59, 2469–2476. doi:10.1016/0016-7037(95)00141-7
641
642